JOURNAL OF MATERIALS SCIENCE **39** (2004) 3293–3308

# Study of surface damage of polypropylene under progressive loading

M. WONG, A. MOYSE
*Polymer Technology Center, Department of Mechanical Engineering, Texas A&M University, College Station, Texas 77843-3123, USA*

F. LEE
*Analytical Division, Atlas Material Testing Technology LLC, Chicago, IL 60613, USA*

H.-J. SUE*
*Polymer Technology Center, Department of Mechanical Engineering, Texas A&M University, College Station, Texas 77843-3123, USA*
*E-mail: hjsue@tamu.edu*

A systematic study of surface damage exerted by a progressive scratching load is performed on model polypropylene (PP) systems. Mar-scratch and stress-whitening transitions can be readily observed, and the corresponding critical loads determined. Distinctive surface damage features are determined before and after the transitions. The progressive load test enables the scratch hardness values to be obtained using the graphical method, thereby allowing scratch resistance to be accurately quantified and ranked among materials. Visibility of the scratched surface is quantified using a gray level analysis *via* a flatbed scanner and a commercial image analysis tool. It is found that the onset of scratch visibility can be determined accurately and reproducibly using the custom-built scratcher under progressive loading condition. Exposed talc particles on the surface of talc-filled PP are found to be responsible for the increased light scattering, leading to greatly increased visibility. The observed scratch visibility is also found to be related to the corresponding friction force profiles. Approaches for producing scratch resistant PP are discussed. 

## 1. Introduction

Scratching is a phenomenon that has been of interest to researchers for many years. In the past, scratches have been investigated as a prelude of wear, which is essentially the consequence of scratching a surface multiple times. Researchers then were more concerned in wear resistance of materials to predict the service life of a component and/or device. Hardness has been recognized as an important factor in wear [1]. However, numerous other factors, such as geometry of contact, velocity of sliding, temperature, lubricant and surface roughness, can be equally important in affecting the tribological behavior of a material system. Scratch testing plays an important role in determining how the above-mentioned factors influence wear resistance.

Scratching and wear of metals and ceramics have been extensively characterized by researchers in the 1950s and '60s [2, 3]. It is known that metals can undergo ironing, ploughing, cutting and fragmentation during scratching, depending on the type of metal investigated and the specific test conditions applied. The dominant mode of damage in ceramics is fragmentation. Polymers present a unique case of scratch behavior. Viscoelastic effects allow polymers to recover quickly after scratching. Scratching of polymer surfaces can often produce different surface features concurrently or sequentially [4, 5]. Fillers and additives can add to the complexity of the surface damage features observed, where stress-whitening often occurs due to the formation of voids, cracks, and exposure of filler particles [6, 7].

Polymers can undergo ironing, ploughing, cutting and fragmentation like metals do. Determination of particular types of damages occurring during scratching is of great concern to tribologists. Ability to identify a criterion or a set of criteria to predict the type of damage features during a scratch process is of paramount importance to polymer materials scientists today. This knowledge has implications in applications where polymers are used as structural or coating materials. Introducing scratches on the surface can result in a drop in fracture toughness of the polymer. In coating materials, delamination will occur if the scratch extends too deep into the coating layer. The severity of the scratch is dependent on the type of scratch damage that occurs. Thus, it is important that polymer scientists know how to predict

*Author to whom all correspondence should be addressed.

scratch behavior to allow significant extension of polymers for applications where surface properties are of prime importance.

Attempts by researchers to classify the different scratch behaviors that polymers exhibit have resulted in the construction of scratching maps [8–10]. The scratching maps allow the prediction of scratch behaviors of specific polymers under specific conditions, such as variations in normal load, scratcher cone angle and tip geometry. Researchers have also sought to identify the many different types of surface damage features observed. Ironing denotes the scratch behavior which results in smooth featureless grooves that are due to plastic or viscoelastic/viscoplastic deformation. When the scratching process moves into the ploughing regime, wave-like patterns [5], cracking [8], plastic drawing [11], and bamboo-like features [4] are some of the damage features observed in polymers. The cause(s) for each type of damage feature can be due to brittle or ductile modes of deformation, or both. The ploughing process is also sensitive to many other factors, such as rate and temperature, which further complicate the efforts to predict such a damage process. Cutting and fragmentation are modes of material removal. Cutting produces ribbons of material in front of the scratching tip and is associated with ductile failure; whereas machining or fragmentation[1] produces fragmented debris from the substrate and is associated with brittle failure [12].

Crazing, shear yielding, microvoiding, cracking and debonding may occur when the polymeric surface is scratched. It was shown by Tang [12] that shear yielding and the formation of shear bands were the dominant form of deformation in rubber-filled polypropylene (PP); Xiang *et al.* [14] came to the same conclusion based on their study on neat polystyrene (PS). Clearly, various types of surface damage phenomena can be observed during scratching of polymers, making it essential for fundamental understanding and prediction of scratch-induced damage in polymers.

An additional problem in the study of scratching on polymers is the multitude of test methods employed. Differences in test conditions and methodology will produce very different scratch behavior and damage features. This concern has been raised by Wong *et al.* [11]. It has been proposed that the progressive load test be employed as a standardized scratch test, which allows for a better link to material parameters and for easier comparison of results. The present work will thus follow the newly proposed [11] test method to study the scratch behavior of polymers.

Another major concern to polymer scientists and engineers is the visibility of scratches on polymer surfaces. Polymers in automotive interior and exterior parts are susceptible to mars and scratches that vastly degrade their appearance. Polymers that exhibit good scratch resistance are highly desirable. Visibility is a complex issue as it involves many different unquantifiable parameters that can affect how a viewer perceives a scratch. Many attempts have been made to quantify scratch visibility by measuring the surface reflectivity of the scratch [14–19]. Due to the diverse techniques employed and the lack of a systematic study to correlate scratch features with visibility [12], the results obtained for one set of studies is often valid only within a set of narrowly defined conditions. It remains to be seen which of these methods, if any, will prove to be the most useful in characterizing scratch visibility.

The main objectives of this paper are (1) to demonstrate the usefulness of the new scratch test method in quantitatively identifying mar-scratch and stress-whitening transitions, (2) to investigate the relationship between the surface damage features observed during scratching and the corresponding friction force profiles, and (3) to show how the observed surface damage can be correlated to material parameters. It is believed that certain surface damage features and transitions can be linked to the materials properties and the stress state the material experiences. The relationship between the surface damage feature and the corresponding visibility, friction force and applied load is established. Approaches for designing scratch resistant plastics are discussed.

## 2. Experimental

### 2.1. Experimental approach and materials

In this study, polycarbonate sheets (Lexan® 9034, GE Plastics) and four PP-based material systems were selected and their compositions are shown in Table I. For the PP systems, the resin and a dark gray coloring pigment were provided and blended by Solvay Engineered Polymers. Plain talc particles, without surface treatment, were provided by Luzenac, Inc. Injection molding of the plaques, having dimensions of 340 mm × 180 mm × 3 mm, was performed by Advanced Composites, Inc. For testing, the plaques were cut and machined into dimensions of 140 mm × 10 mm × 3 mm. All test specimens were prepared according to ASTM D618-00 Procedure A [20].

A custom-built machine as described elsewhere [11] was used in the testing. A constant scratch speed of 100 mm/s with a linear increasing normal load ranging from 5 to 50 N was performed. The scratch length was set to be 100 mm and tests were conducted at room temperature. A stainless steel spherical ball with a diameter of 1 mm was used as the scratch stylus tip.

Selected samples of the scratched specimens were immersed in water and sonicated for 30 min in a

TABLE I Composition of material systems

| Material system | Material type | Filler (wt%) | Coloring compound (wt%) |
|---|---|---|---|
| 1 | Lexan® | – | – |
| 2 | Homopolymer PP | – | 2NCA (2%) |
| 3 | Homopolymer PP | Talc (20%) | 2NCA (2%) |
| 4 | Copolymer and PP blend | – | 2NCA (2%) |
| 5 | Copolymer and PP blend | Talc (20%) | 2NCA (2%) |

[1]Some authors use the term micromachining to describe machining at very small scale.

Bransonic® ultrasonic cleaner with an output power of 70 W at 42 kHz. The energy generated by the ultrasonic vibration is expected to remove preferentially the remnants from inside of the scratch groove where the material was highly deformed and damaged. The use of this technique will thus help reveal the regions where severe surface damage occurs.

## 2.2. Scratch damage evaluation and quantification

Scanning electron microscopy (SEM) was performed to study the microscale surface damage features using a Jeol JSM-6400 system. A flatbed scanner with a resolution of 1,200 dpi was used to scan the scratched surfaces, to quantify scratch damage. A commercial image analysis tool, VIEEW®, was also used to quantify the surface damage of the specimens.

Quantification of damage was performed in accordance to our earlier method where the scratch width was defined as the distance between the peaks of the two grooves on the two sides of the scratch path [11]. Thin sections were prepared for optical microscopy (OM) observation, under cross-polarized light, using a BX60 Olympus® microscope.

A scratch groove on a given material affects the visibility by altering the light reflected off the surface [21]. The reflected light can be separated into two components, namely, diffuse and specular reflection. The diffuse component is responsible for the perception of color and light intensity. Thus any changes in color and light intensity due to scratching, for example, stress-whitening, can be measured by detecting the changes in diffuse reflection. The specular component is responsible for gloss of a surface. Any changes in surface roughness and topography will affect gloss. A commercial image analysis tool, VIEEW®, was used to investigate scratch visibility in the present work. The commercial image analysis tool has the capability to produce ideal diffuse light *via* red, green and blue light-emitting diodes (LED). The amount of color in the diffuse light can be controlled precisely by changing the intensity of the LEDs. This is useful in characterizing any stress-whitening that occurs. In this experiment, the green and blue LEDS are set at 19.17 and 30.57%, respectively. It was observed that the stress-whitened areas in PP were most distinct under these conditions. VIEEW® can also produce a beam of white light projecting 90° onto the surface. By measuring the light that is directly reflected back, the machine is able to detect edges of the scratch groove, thereby providing an accurate measure of scratch width. In this research, VIEEW® was used to define the locations and areas that were stress-whitened during scratching. The onset of stress-whitening, which can be defined as the light intensity that reaches a predetermined threshold value, could thus be measured reliably. The scratch area is first observed visually and the threshold value is adjusted until it matched the area from visual inspection. Then, this value is further correlated to the friction force profile to ensure accuracy. The corresponding critical distance, and consequently critical load, can be obtained *via* this method. For scratch visibility evaluation *via* scanner, the scratched specimens were scanned together against a piece of white paper. The scanned image was then processed by adjusting brightness and contrast of the image so that the piece of white paper in the image had a value of 255 in grayscale. The gray level of the image was then measured using Scion Image Beta 4.0.2. The length of the scratch groove was divided into five equal sections, each with 20 mm in length. Fig. 1 shows the gray level plot of two specimens that were scanned together. The values shown are the average gray level along the scratch groove within the 20 mm section. The peaks (indicated by arrows) show that higher amounts of light were reflected off the scratch groove than the surrounding areas.

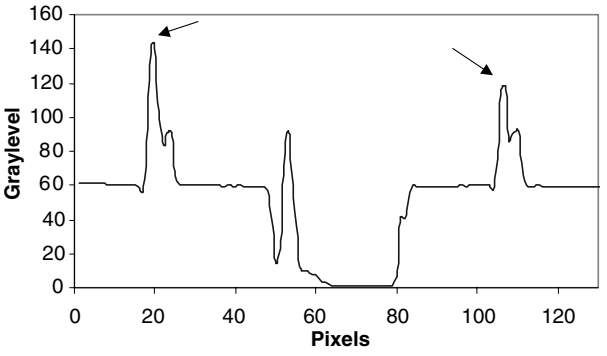


*Figure 1* Gray level plot of scratch groove from scanner image.

## 2.3. Indentation hardness, scratch hardness, and friction coefficients

Hardness has been widely utilized to make correlation with scratch resistance [22]. In an indentation hardness test, where a spherical indenter is applied under constant load on to a smooth surface of a perfectly plastic material, the Meyer hardness is defined as the ratio of the load, $W$, to the projected area of the indentation. Thus, if $d$ is the diameter of depression left behind after the indenter has been lifted away from the surface, the Meyer hardness is given as [23]:

$$H_{\mathrm{M}} = \frac{4W}{\pi d^2} \tag{1}$$

This relationship is true even for indenters of conical or pyramidal geometry. For metals and ceramics, load and depth are found to obey the following relationship,

$$W = kd^{\mathrm{n}} \tag{2}$$

Equation 2 is known as Meyer's law, where $k$ and $n$ are constants to be found for the material being studied, and $W$ and $d$ are the indentation load and the diameter of the residual indented area, respectively. In an ideal situation $n = 2$ and thus hardness remains constant with load. For metals and ceramics, the value of $n$ may be less than 2, and for many soft materials it is found to lie between 2 to 2.5 [23]. Many authors have found that $n = 2$ for glassy polymers, such as poly (methylmethacrylate) (PMMA) [24, 25] and polystyrene (PS) [26]. Similar results were also found for semicrystalline polymers, such as PP [27]. Indentation size effect is the

phenomenon of depth-dependent hardness of materials especially at shallow depths. It was observed that hardness values are higher at very small indentation depths in metals. Indentation size effect in metals is explained by the interactions of dislocations in crystalline materials resulting in the strengthening effect [28, 29]. A reverse indentation size effect has been reported in polymers and it has been suggested that the presence of a thin layer of polymer with lower $T_g$ results in lower hardness values at very shallow depths [30, 31]. In spite of the range of values shown in $n$, elastoplastic models of indentation based on a simple quadratic relationship have been utilized to fit many materials successfully [32]. A model that proposes a more complicated relationship between load and depth was utilized to describe the effect of work-hardening and creep [33].

Scratch hardness is defined as the normal load of the indenter over the projected load bearing area. It is normally taken to be equivalent to the indentation mean pressure exerted on the material during scratch. For a viscoelastic-plastic material, such as a polymer, elastic recovery is almost instantaneous and the load bearing area can be approximated as a circle with its diameter the same as the scratch width. It should be noted that this assumption is based on the fact that PP is well known to undergo large elastic and viscoelastic recovery [14]. Thus scratch hardness $H_s$ can be defined as

$$H_s = \frac{4W}{\pi d^2} \tag{3}$$

where $W$ is normal load and $d$ is scratch width. It was also argued by Briscoe *et al.* [9] that viscoelastic recovery of polymers does not affect scratch width significantly. Thus it is reasonable to measure the scratch width after the test to obtain scratch hardness.

In this work, progressive load tests will be conducted on the specimens instead of the commonly used constant load tests. Scratch hardness is defined as the ratio of the change in normal load, $W$, over the change in projected area, $A$.

$$H_s = \frac{\Delta W}{\Delta A} \tag{4}$$

Projected area can be found by measuring the scratch width, $d$, and using the equation:

$$A = \frac{\pi d^2}{4} \tag{5}$$

Thus, if scratch hardness is constant at different loads, the graph of normal load, $W$, against projected area, $A$, will give a linear plot and its slope will be equivalent to its scratch hardness. It should be noted that the form of the equations used in scratch hardness and indentation hardness are identical. If Meyer's law holds true for scratch hardness as it is for indentation hardness, we should expect that for polymers, $H_s$ is constant for different loads since $n = 2$. One of the objectives of this paper is to evaluate whether or not scratch hardness is a sensible parameter to quantify scratch resistance of polymers.

The ratio of tangential force, $F$, over the normal load, $W$, is herein defined as the scratching coefficient of friction, $\mu_{sc}$ [34]

$$\mu_{sc} = \frac{F}{W} \tag{6}$$

This is to distinguish the parameter obtained using this test method as opposed to the coefficient of friction normally found by the sliding of two planar surfaces.

## 3. Results and discussion

### 3.1. Scratch hardness

Scratch widths of the scratched specimens of the four model PP systems and polycarbonate were measured from VIEEW® direct-light images. The definition of scratch width used here was discussed in our previous paper [11], Fig. 2 gives an illustration of the definitions used. Since the materials used in the current study exhibit prominent pile-ups on the side of the scratch groove (see Fig. 5), the scratch widths measured by VIEEW® are equivalent to SW1, as defined in Fig. 2. Scratch widths from the initial and the end regions of the scratch grooves were ignored due to the unstable nature of the scratch head movement in those regions. The projected load-bearing area is then calculated according to Equation 5. The resultant graphs of normal loads against projected load-bearing area were plotted as shown in Fig. 3. The resultant plots give very good linear fits as was predicted earlier. The slope is easily determined, and the results are listed in Table II. It is noted that all the plots do not begin at the zero origin. This is attributed to the initial load coming from the dead weight of the stylus. If initial load is zero, the resultant graph will begin at the origin. However, if the initial load is greater than zero, the graph will be shifted upwards, as is observed in Fig. 3. Errors

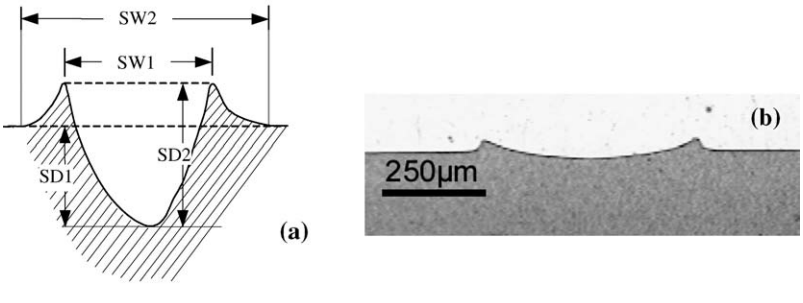


*Figure 2* (a) Definitions of scratch widths and scratch depths; (b) Actual cross section.

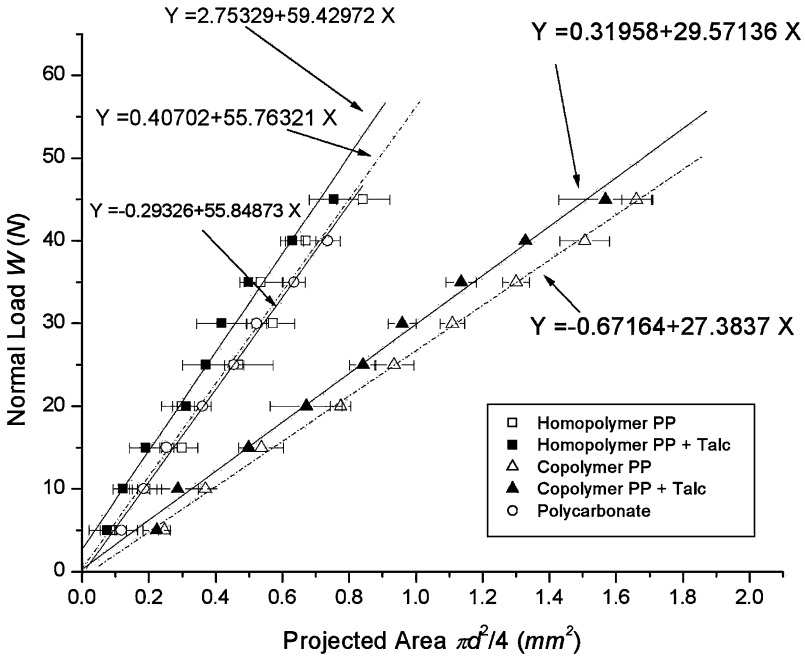


*Figure 3* Graphical method of obtaining scratch hardness.

will also likely be induced when measuring the scratch widths which will result in the horizontal shift of the plot. As it is the slope of the graph that gives scratch hardness instead of individual data points, the exact location on the scratch cross-profile where scratch width is measured is not important, as long as the series of points along the longitudinal direction of the scratch groove of which scratch widths are measured is consistent. This eliminates the requirement to use expensive 3D profilometers or time-consuming cross-sections of the scratch to obtain the scratch width. A 2D scan of the scratch groove will give a reliable scratch hardness. Thus, despite the inherent errors introduced during the experiment, the slope of the plot, i.e., the scratch hardness can still be obtained consistently. This value of scratch hardness, although not entirely free of errors, is an improvement over the conventional method of obtaining scratch hardness, whereby a scratch at constant load is performed and scratch width measured to obtain the scratch hardness. The proposed method gives a more representative value as it is derived from a range of loads as opposed to the single constant load used in the conventional method.

It is known that stick-slip may occur during scratch. Stick-slip involves the buildup of stress and gross plastic deformation in front of the scratch tip, followed by a sudden release of strain energy that creates distinct features that can be observed easily. Stick-slip will result in local variation of scratch width such as that shown in Fig. 4. However, it seems that this local variation does not affect the overall trend in scratch width variation.

Skin-core morphology is formed in injection-molded thermoplastics. A faster cooling rate exists next to the colder mold surface. This induces a nearly amorphous skin preferentially, whereas large crystallites and, possibly, spherulites are formed in the core of the bulk polymer. A transition zone exists between skin and core that is composed of smaller spherulites. The cross-polarized optical micrograph shown in Fig. 5 illustrates a typical skin-core morphology in all of the systems used. The above-mentioned zones are indicated in the micrographs. It is also well-known that the crystalline polymer phase is harder than the amorphous phase [35]. As the scratch stylus gouges deeper into the bulk, the corresponding scratch hardness might change. Again, this does not seem to have led to any significant variations in the plot shown in Fig. 3 for obtaining scratch hardness. Thus, despite the presence of stick-slip and skin-core morphology, the scratch hardness values can still be reliably obtained, and the robustness of the graphical method in determining scratch hardness is demonstrated. It should be cautioned that if the skin thickness of the skin-core morphology is smaller than, or close to, the scratch depth, the slopes of the scratch hardness curves may begin to change (Fig. 3). Therefore, it is advised that microscopy be utilized to check the thickness of the skin morphology for a given set of injection molded part before the scratch hardness of the samples is determined.

The scratch hardness values as shown in Table II shows the effect of talc on scratch hardness unequivocally. Talc increases scratch hardness in both homopolymer and copolymer PP systems. This is in reasonable agreement with the conclusion found in comparing the mechanical properties of the PP systems (Table III). It is interesting to note that the present

TABLE II Scratch hardness obtained from graphical method

| Material | Scratch hardness (MPa) |
|---|---|
| Lexan® | 55.8 |
| Homopolymer | 55.8 |
| Homopolymer + Talc | 59.4 |
| Copolymer | 27.4 |
| Copolymer + Talc | 29.6 |

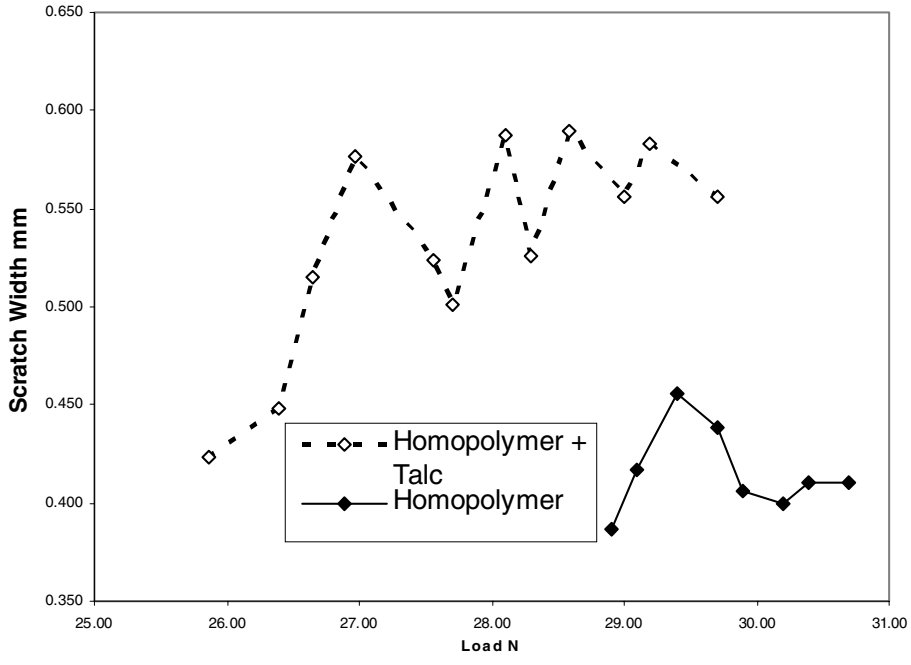


*Figure 4* Scratch width of regions shown in Figs 5 and 6. Spikes denote stick-slip events.

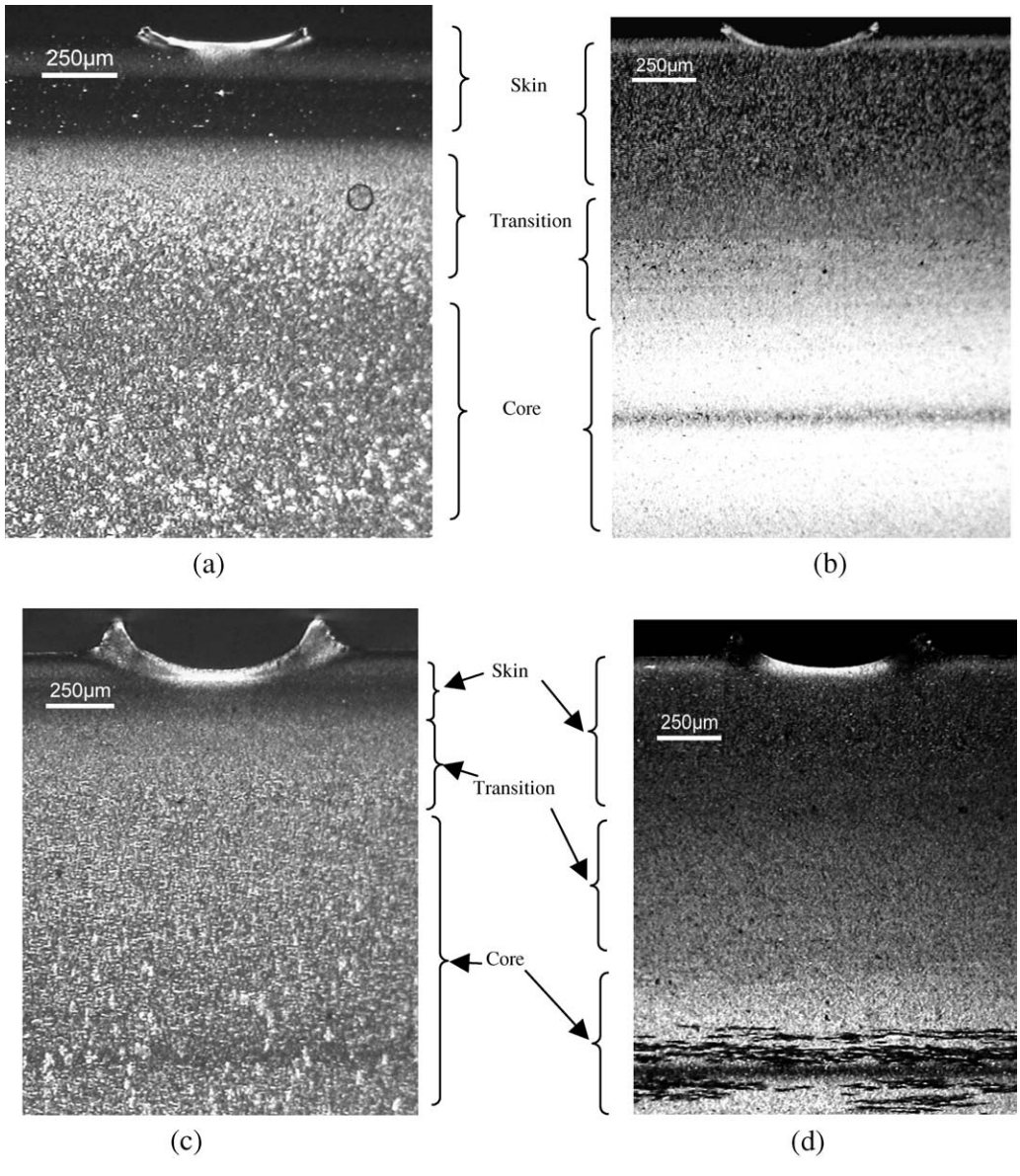


*Figure 5* Skin-core morphology of (a) homopolymer, (b) talc-filled homopolymer, (c) copolymer and (d) talc-filled copolymer. Note that the cross-section of scratch groove on each surface corresponds to that at 30 N normal load.

TABLE III Mechanical properties of material systems

| Material | Tensile modulus (GPa) | Yield strength (MPa) |
|---|---|---|
| Lexan®[a] | 2.38 | 62 |
| Homopolymer | 1.73 | 33.47 |
| Homopolymer + Talc | 2.73 | 35.30 |
| Copolymer | 1.07 | 22.55 |
| Copolymer + Talc | 1.55 | 23.28 |

[a]Mechanical properties reported from manufacturer data sheet.

homopolymer PP systems have comparable scratch hardness to polycarbonate.

It should be noted that scratch hardness values are an indicator of the resistance of a material against permanent surface deformation. This information is useful for determining the residual strength of the polymer surface against loading after being scratched. The scratch hardness values may also be used to predict scratch induced visibility. However, care has to be taken to make sound correlation indicated above. The nature of the permanent surface deformation and damage has to be determined before the above correlation can become meaningful [14]. This leads to a need to find out the exact surface damage feature after scratching, as will be discussed below.

## 3.2. Homopolymer surface features

Figs 6 and 7 show the scanned images of PP homopolymer and talc-filled homopolymer scratched under progressive loading. Various regions of interest are highlighted, and SEM micrographs of these locations are also displayed in Figs 6b–e and 7b–e. In Fig. 6, Region 1 shows the characteristic wave-like deformation, which is similar to PP scratched under low loads and low speeds [35–38]. It has been shown by Tang and Martin [13] that these wave-like patterns are likely to be the result of shear bands formed near the surface of the scratch groove. Region 2 shows a transition

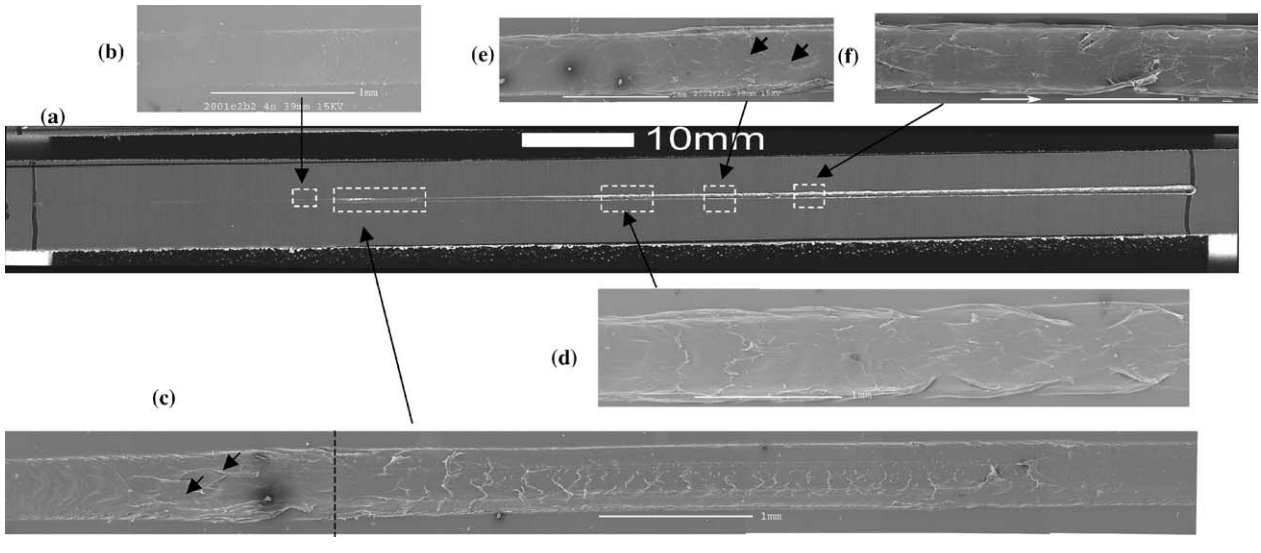


*Figure 6* (a) Scanned image of scratched homopolymer, (b) region 1, (c) region 2, (d) region 3, (e) region 4 and (f) region 5 are SEM micrographs of highlighted regions in the scratch groove. Note that region 5 shows fibril breakage after sonication.

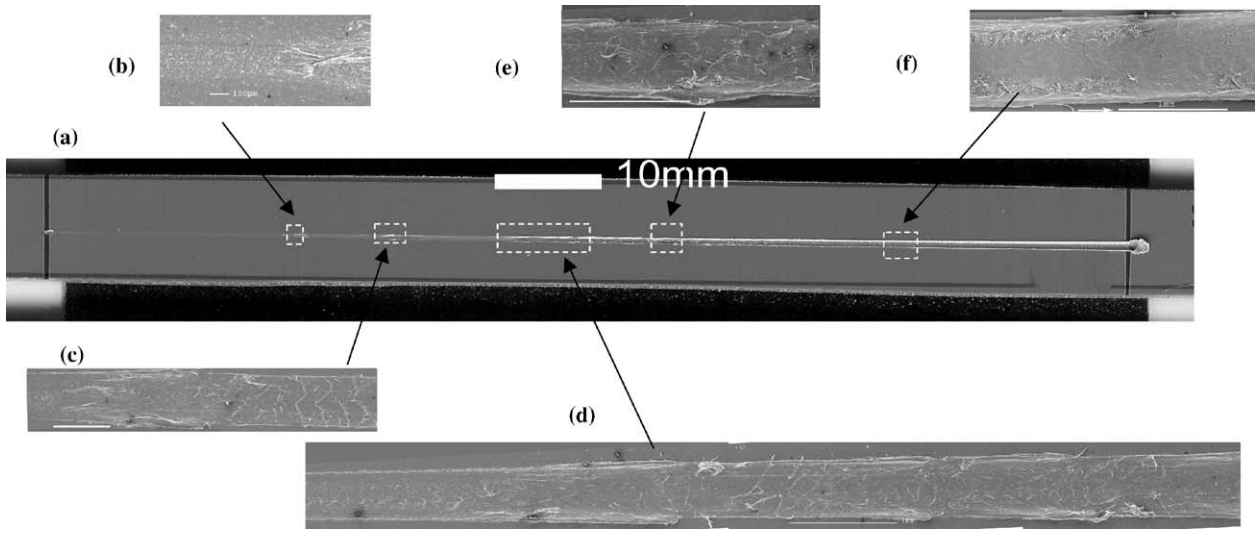


*Figure 7* (a) Scanned image of scratched talc-filled homopolymer, (b) region 1, (c) region 2, (d) region 3, (e) region 4 and (f) region 5 are SEM micrographs of highlighted regions in the scratch groove. Note that region 5 shows fibril.

in damage feature. The width of the groove increases more rapidly. The regular parabolic lines are no longer present, and are replaced by irregular brittle type of failure. This suggests that shear banding is no longer the major mode of deformation. Fracture lines are clearly visible, which are indicated by the arrows shown in the micrograph. The scanned image also shows an increase in visibility because of the increase in whiteness of the groove. Interestingly, the damage pattern settles into a regular sigmoidal pattern after it has reached the maximum width (indicated by dashed line) and gradually fades away into a smoother groove. Region 3 shows another type of transition. In this case, damage becomes more severe and the deformed material forms 'lips' that overflow to the side of the groove. This indicates an increase of pileup in the scratch groove. In the later stage of the scratch, surface damage is predominantly random fracture lines (indicated by arrows). Regions 4 and 5 show that the damage features remain unchanged. Region 5 was subjected to sonication before SEM analysis to remove remnants from the scratched surface. An anomaly that is attributed to the sonication process is observed in Region 5. More on this anomaly will be discussed in a later section.

Fig. 7 shows a similar progression in severity of surface damage of a talc-filled homopolymer. However, there are some obvious differences. Firstly, a clear transition from mar to scratch is seen in Region 1. The surface damage is barely perceptible before transition except for a slight difference in surface texture from the unscratched surface. After the transition, a dramatic change in damage mode occurs with large plastic drawing. Region 2 shows a very similar type of transition as shown in the homopolymer case. Region 3 shows a rougher surface with debris (encircled in white), in contrast to the relatively smooth surface in Fig. 6. It is observed that a segmented type of damage pattern appears in region 3, which suggests the occurrence of a stick-slip process. In region 4, the scratched surface shows a very rough texture with debris, fibrils and large pileups on the side. Thus, the evidence seems to suggest that the addition of talc affects the damage mode during scratch by inducing extensive localized plastic deformation. Region 5 was subjected to sonication like in the previous example. Again, the anomalous features found are attributed to the sonication process, and will be discussed later. The microscopic damage features observed in the scratch grooves of both homopolymer and talc-filled homopolymer suggest that a certain sequence of deformation process has taken place, allowing for fundamental understanding and correlation of the formation of such damage to the applied load and material parameters.

### 3.3. Homopolymer friction force profile

Fig. 8a and b show the friction force profiles for the specimens displayed in Figs 6 and 7, respectively. Tangential force as measured by the scratch machine is represented by solid lines, while scratching coefficient of friction is represented by dashed lines. The scratching coefficient of friction shows a gradual increase as the scratch distance and normal load increases. A similar increase in scratching coefficient of friction was observed in polycarbonate by Rats *et al.* [39]. In their experiments, a Rockwell C type stylus was used to scratch polycarbonate over a load range from 0 to 10 N.

The friction force profile is characteristically marked by fluctuations that are obviously due to the irregularities encountered during scratching. If the distances, as represented by the dashed vertical lines in the plots, that correspond to the highlighted regions shown in Figs 6 and 7 are marked on the friction force profile, we can see spikes in some of them. Regions 2 and 3 of Fig. 6 and Regions 1, 2 and 3 of Fig. 7 correspond to large spikes in the force profile. Reviewing the SEM micrographs will show that the transitions are sudden, signifying a change in damage mode. This clearly shows the ability of this method to capture important friction force data that relate to the physical damage features generated during scratch.

The scratching coefficient of friction is calculated from the linear increase in normal load and the tangential force recorded, using Equation 6. This second plot is useful in contrasting the spikes and fluctuations that exist in the friction force plot. The plot is marked initially by instabilities that occur during the start of the scratching process, hence resulting in exaggerated spikes as seen in the plot. The graph stabilizes rapidly and produces a predictable trend. It is noted that there seems to be distinct regions in the profile as scratching progresses. The first region denotes a gradual increase in friction coefficient. The curve then approaches a flatter slope, followed by another change in slope in the last part of the curve. This plot when coupled with the observations in the SEM micrographs suggests that the varying rate of increase in scratching coefficient is the result of different physical damage mode occurring during scratching. However, it should be cautioned that the above results should not be construed as evidence that the profile actually increases linearly in each phase, nevertheless it serves as a useful tool in understanding the scratch behavior. For comparison purposes, the friction force profile of a polycarbonate specimen is shown in Fig. 9. The scratch groove of the polycarbonate specimen showed no transition at all, and smooth ploughing took place over the entire scratch length. The scratch test for polycarbonate was performed under identical conditions as PP. The friction force plot shows a smooth, nearly constant slope over the entire scratch process.

### 3.4. Copolymer surface features

The friction profiles of the scratched PP system thus seem to show a behavior that is incongruent with any previously known theory. To explain the apparent change in the slope of the scratching coefficient, copolymer and talc-filled copolymer systems were sonicated. It is hypothesized that localized regions of the scratched surface are highly strained during scratching; a controlled burst of energy supplied by the vibration of water during sonication might be able to "dust-off" remnants of loosely attached damage in

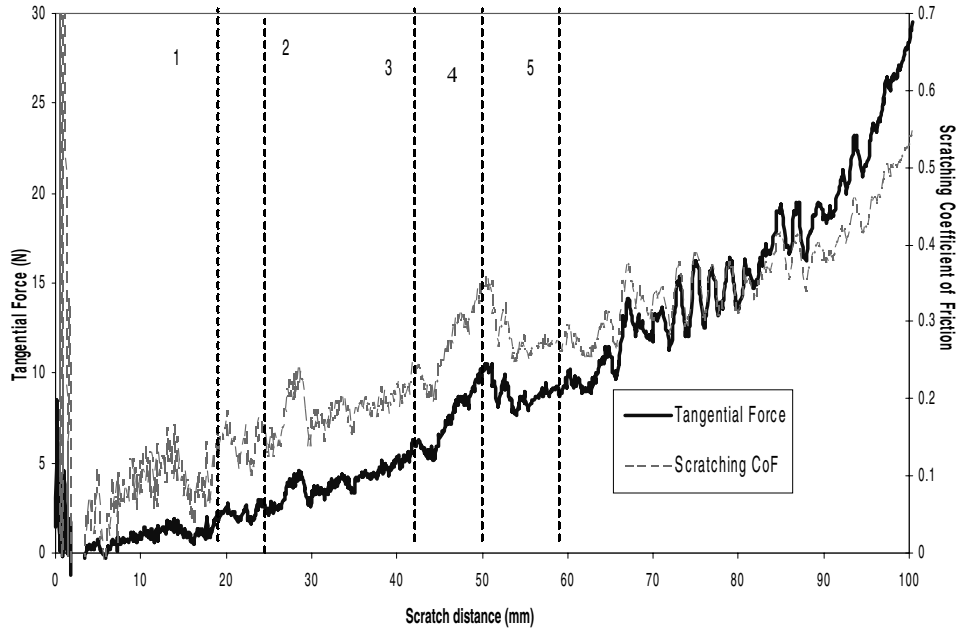


**(a)**

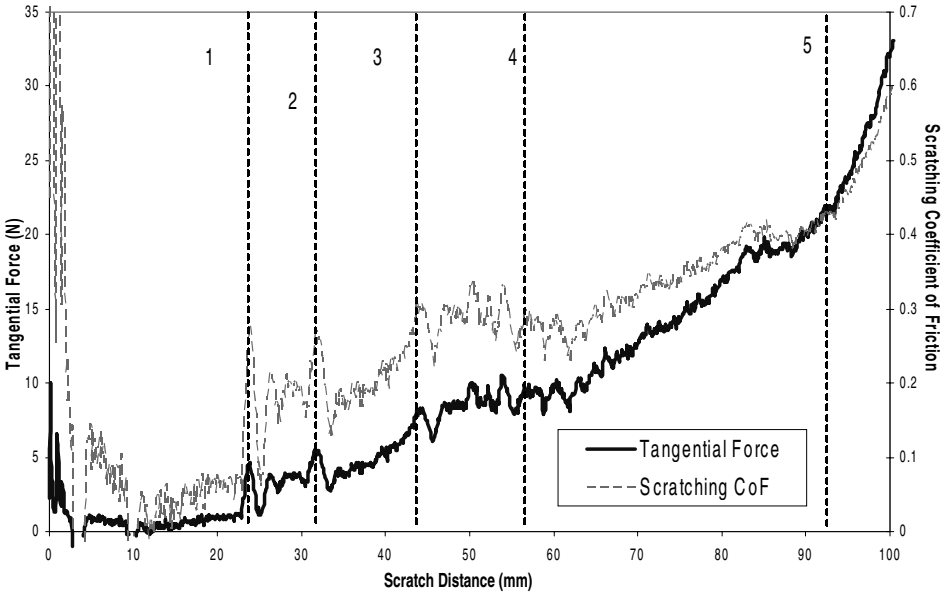


**(b)**

*Figure 8* Friction force profile from scratch test of (a) homopolymer and (b) talc-filled homopolymer.

these regions. It was hoped that the copolymer systems, having a lower stiffness and higher ductility, will show sonication-induced failure more readily. Copolymer does not show any induced damage feature from the sonication (Fig. 10). Region 1 shows a gradual transition from regularly spaced wave-like lines, due to formation of shear bands, to irregular deformation lines. Region 2 shows extensive deformation that marks the beginning of the stress-whitened zone.

Talc-filled copolymer, however, shows a very different surface feature after sonication. Fig. 11 shows the appearance of pits on the surface that correspond to highly visible marks in the scanned image. The pits exhibit remnants of broken fibrils at the edges. The pits appear to be made of concentric circles of layers of polymer. In fact, the step-like feature allows easy counting of the number of layers in each pit. As the scratch progresses, the pit grows by increasing the number of steps. Eventually the pits give way to large-scale failure that creates the feature seen on the right of the pits. It is of significance to note that the substrate material forms layers, each with a different amount of stretching during the scratch process. It is proposed that this process is similar to the biaxial stretching of polymer films. The highly damaged zones are concentrated in well-spaced, nearly spherical regions, which manifest as pits after sonication. The inter-pit distance is plotted in Fig. 12. It is apparent that inter-pit distance increases with increasing scratch distance, which accounts for the larger deformation observed as the scratch distance and the scratching loads increase.

Encouraged by the results shown in talc-filled copolymer, the homopolymer systems were revisited and sections that correspond to the later portion of the

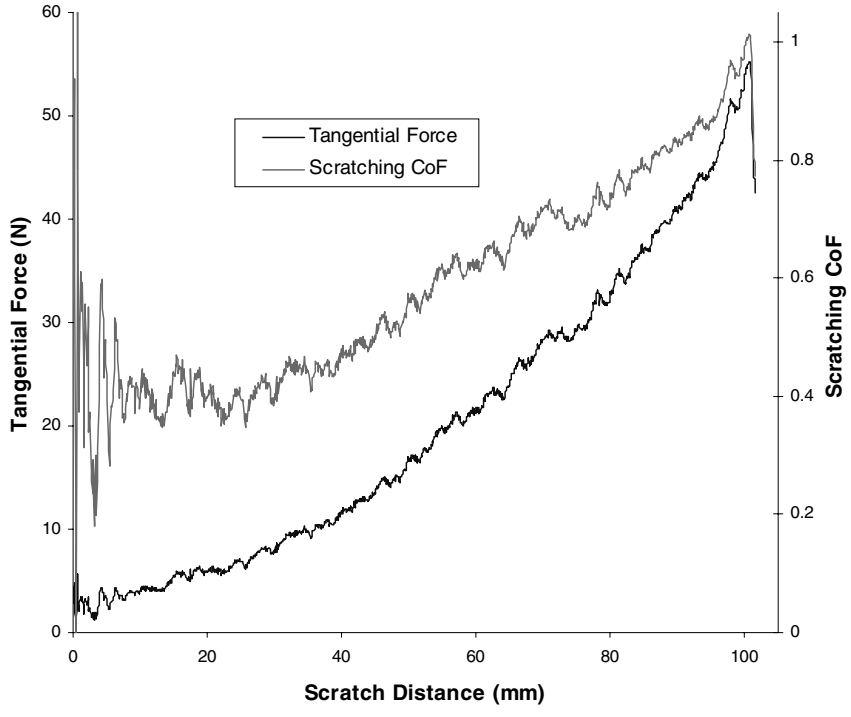


*Figure 9* Friction force profile of PC showing nearly constant slope in both curves.

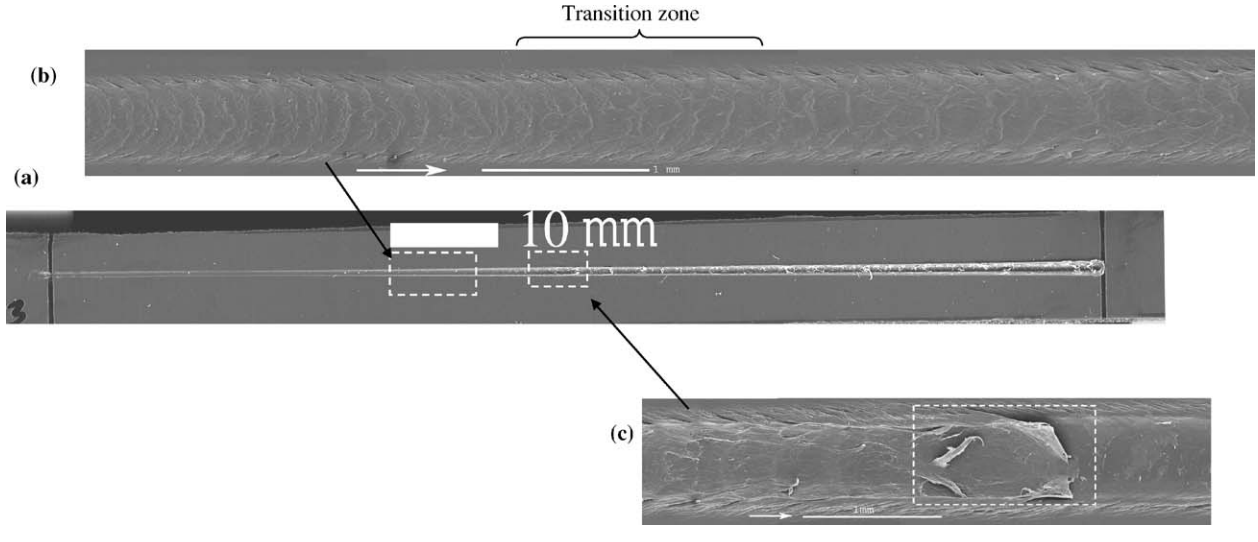


*Figure 10* (a) Scanned image of scratched copolymer that was sonicated, (b) region 1 and (c) region 2 shows extensive deformation indicated by box.

scratch were also sonicated. It is anticipated that sections under higher loads should provide a better chance of showing highly strained regions. However, only remnants of broken fibrils were formed on the sidewalls of the groove (Figs 6f and 7f). This indicates that the highly strained region in homopolymer is on the side of the groove, which is in contrast to copolymers where the most strained regions are at the center of the groove. Fig. 13 shows the formation of highly stretched fibrils in homopolymer and talc-filled homopolymer, respectively. The presence of fibrils offers another explanation to the observed change in the slope of the friction force profile of PP. Fibrils are formed during the cold-drawing of the polymer. Fig. 14 shows a tensile engineering stress-strain curve typical of talc-filled copolymer PP that yields and cold-draws. Cold-drawing occurs within the plateau region [40]. It can be seen that stress remains relatively constant while strain increases dramatically within this region. The amount of tangential force required to move the scratch stylus may drop due to cold-drawing.

## 3.5. Copolymer friction force profile

Friction force profiles for the copolymer systems are in general similar to those of homopolymer systems. Four distinct regions can be seen, and they behave in a similar manner as mentioned in Section 3.3. Fig. 15 shows the friction force profiles of copolymer and talc-filled copolymer, respectively. Regions 1 and 2 shown in Fig. 10 are marked in Fig. 15a. Region 2 shows a spike that corresponds to the observed deformation event. Fig. 15c shows the detailed profile of Fig. 15b that corresponds to the surface features observed in Fig. 11b. Each dashed line in the cluster of lines on the left of the

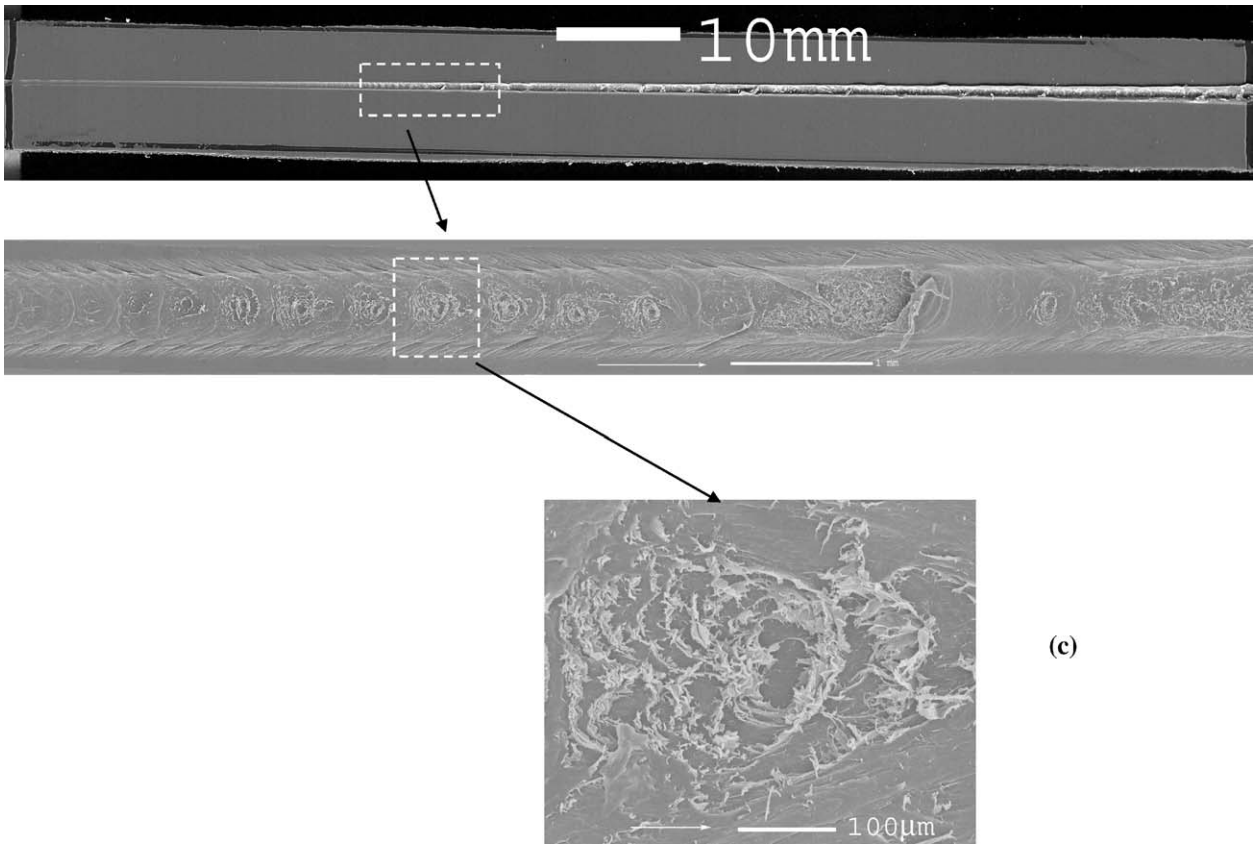


*Figure 11* (a) Scanned image of scratched talc-filled copolymer that was sonicated, (b) region 1 and (c) close up of a pit in region 1.

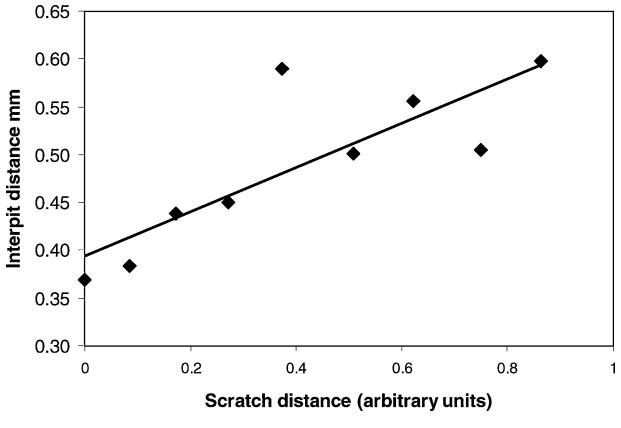


*Figure 12* Inter-pit distance shows an increase against scratch distance.

graph indicates a pit observed in the SEM micrograph. It can be seen that each pit corresponds to a peak in the friction force profile. There is an unaccounted spike in between the ninth and tenth line that does not appear to correspond to any physical feature observed. The two larger peaks on the right of the graph correspond to the two large-scale deformation regions observed in the SEM. Thus, the above results further corroborate that the pits are the highly strained regions. The fidelity of the friction force profile to the SEM micrographs has also been confirmed by this study.

## 3.6. Scratch visibility

### *3.6.1. Stress-whitening*

It is well-known that crazing produces voids which could contribute to stress whitening. Rengarajan *et al*. [41] found that PP which contains impact modifiers that promotes shear deformation exhibits less stress-whitening than PP containing impact modifiers that promote crazing and void formation. Tang and Martin [13] provided evidence of void nucleation from the rubber phase in rubber-modified PP. The current copolymer actually contains a rubber phase, and thus stress-whitening can occur either by voiding or crazing induced by the rubber phase. This explains why the copolymer system has a lower critical load to onset of stress-whitening. A smaller rubber particle size, a stronger rubber-matrix bonding and a higher cavitational strength of rubber may reduce the nucleation of voids and stress-whitening.

Talc, if not properly treated, is well-known to increase stress-whitening of polymers. The SEM micrograph in Fig. 16 shows exposed talc particles after scratching at 30 N and 100 mm/s in the homopolymer. Fig. 17a shows an image that was obtained from VIEEW®. Blue and green diffuse lights were used during the scanning of the images as it was found that visibility of the scratch grooves in talc-filled systems was most prominent at these particular light wavelengths. Holoubek *et al.* [7] showed that in a stress-whitened PP, light scattering due to voids is relatively insensitive to different wavelengths of the visible light, whereas, light scattering due to ethylene-propylene-diene monomer (EPDM) rubber particles embedded in PP is most effective at wavelengths around 400 nm (violet), which gradually drops off as wavelength increases. Although talc particles, not EPDM particles, are present in the talc-filled homopolymer PP, the fact that scratch visibility is sensitive to wavelength of light suggests that

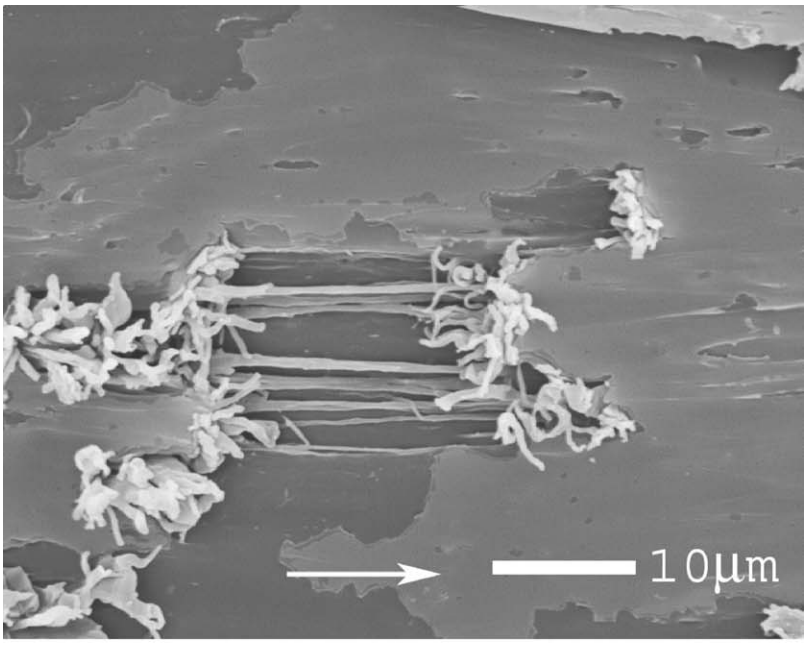


(a)

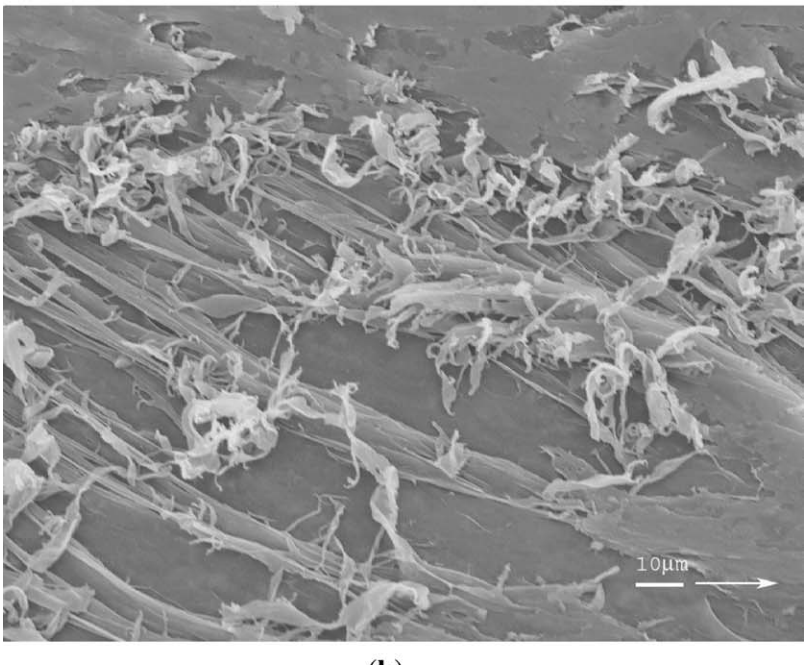


(b)

*Figure 13* Fibrils in (a) homopolymer and (b) talc-filled homopolymer.

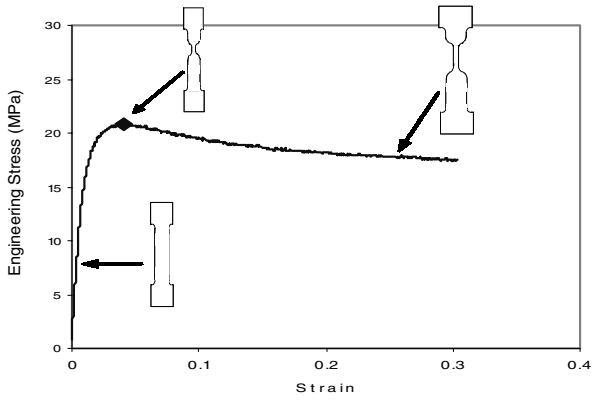


*Figure 14* Engineering stress-strain graph of talc-filled copolymer PP that yields and cold-draws.

talc plays an important role in causing such pronounced increase in scratch visibility.

The white-colored region in Fig. 17a represents the area that has been stress-whitened. The procedure of defining stress-whitening was described earlier in Section 2.2. When this image is superimposed onto the friction force profile, a correlation between the onset of stress-whitening and a steep drop in friction force is easily seen. This coincidence in onset of stress-whitening and drop in friction force is observed in all polymer systems except for homopolymer PP and PC, where no appreciable stress-whitening was detected. Another feature that seems to be recurring is the higher probability of large amplitude fluctuations in the friction force curve pattern that manifests

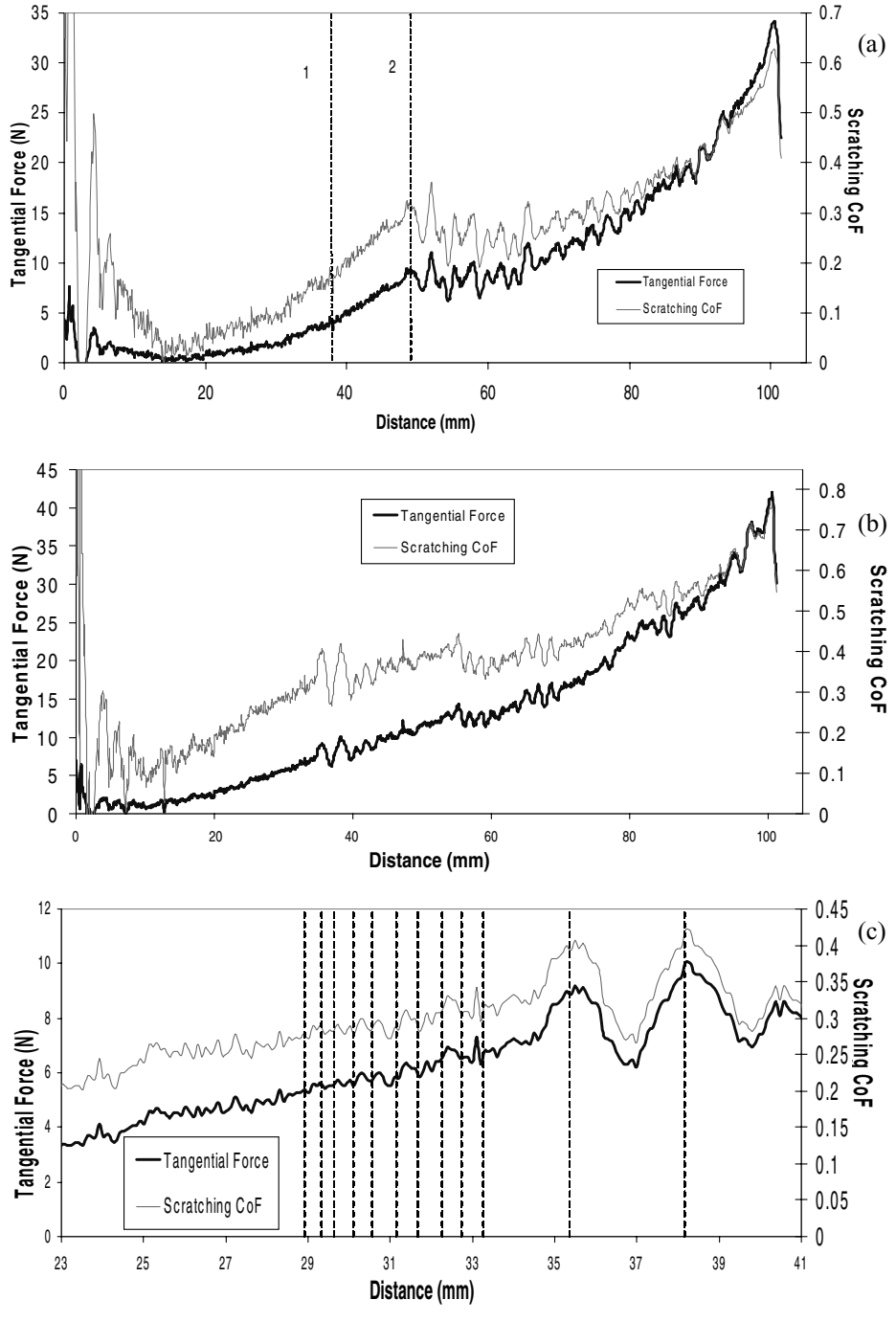


*Figure 15* Friction force profile from scratch test of (a) copolymer and (b) talc-filled copolymer. (c) shows the detailed profile of (b) that corresponds to Fig. 11b.

after this steep drop in friction. The large fluctuations would seem to suggest that the damage mechanism has changed such that a smooth sliding motion across the surface becomes less likely. Yielding, fracture or stick-slip events as evidenced in the earlier micrographs are possible reasons for the observed fluctuations. The drop in friction is probably a result of a sudden failure by yielding or fracture, which can result in the formation of voids or the forced exposure of talc particles. These observations provide a useful criterion in defining the initiation of stress-whitening in PP. It has been suggested that talc particles in PP play no role in shear band formation during scratching [13]. In the present case, the presence of talc particles aggravates the damage by debonding at the particle-matrix interface and matrix drawing, as seen in Figs 7 and 16.

A set of three specimens from each material was scanned using the VIEEW® system. The critical load to onset of stress-whitening was obtained, and the results are given in Fig. 18. The results show that for the PP systems, the magnitude of critical load to stress-whitening occurs in the following descending order: homopolymer, talc-filled homopolymer, copolymer, talc-filled copolymer. We see that scratch visibility is partly dependent on mechanical properties, such as tensile modulus and yield strength (Table III). Lower moduli and lower yield strength give a lower critical load for the transition to take place. Fig. 19 shows the size of the area that was stress-whitened for each material system.

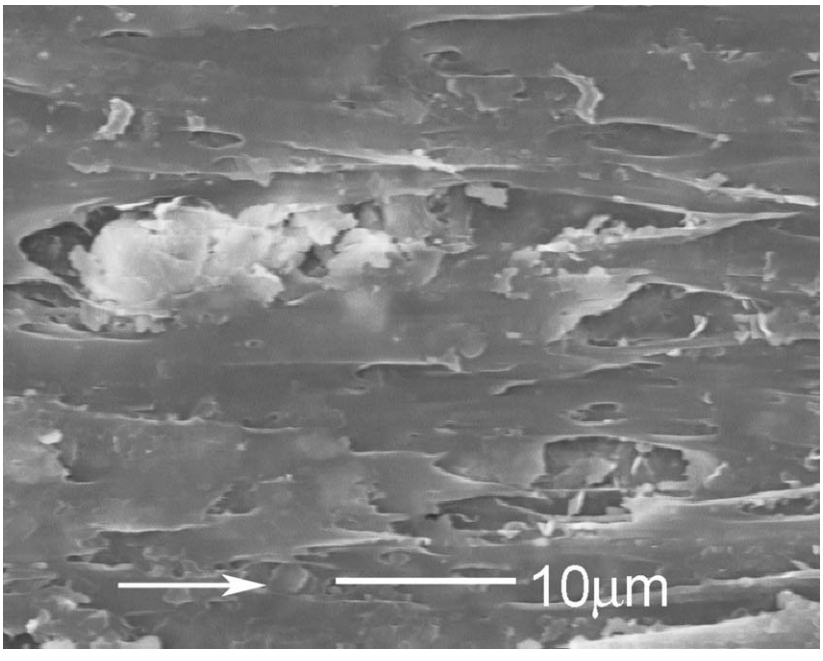


*Figure 16* SEM micrograph of exposed talc particles in a talc-filled homopolymer. Arrow indicates scratch direction.

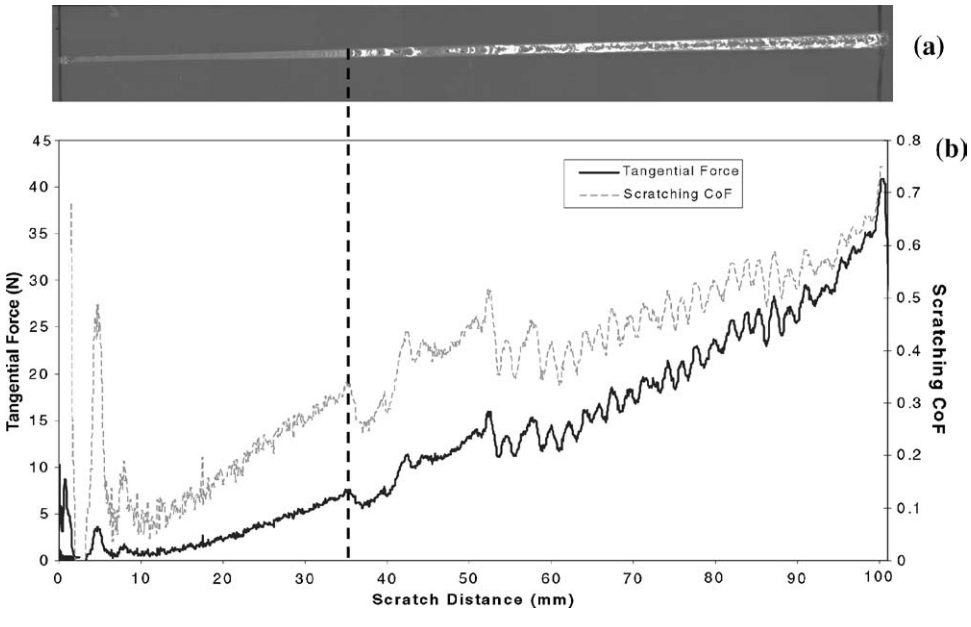


*Figure 17* (a) Image from VIEEW®, white region indicates stress-whitening, (b) friction force profile for this talc-filled copolymer specimen, dashed line shows excellent correlation with onset of stress-whitening.

Talc-filled polymers show a larger affected area. It is apparent that untreated talc not only decreases the critical load to stress-whitening, it also dramatically increases the amount of stress-whitening.

The evidence presented points strongly to the role of filler particles in scratch visibility. It is thus proposed that the main reason for the difference in scratch visibility between the current PP materials studied is the tendency of the material to form light scattering voids or exposed talc particles at the critical load. Logically, this critical load will probably be related to some yielding or fracture criteria, depending on the specific failure mode that occurred. To illustrate this point, homopolymer is found to fail by fracture without any observable void formation (Fig. 6). On the other hand, talc-filled homopolymer fails *via* debonding of talc particles and drawing of the matrix as evidenced. Voids and debonding occur as a direct consequence of this change in damage mode, and these are the causes for significant light scattering. Accordingly, for homopolymer PP, it is suggested that minimal stress-whitening will take place as long as the failure mode does not change.

Scratch hardness and scratch visibility are two major components in defining the scratch resistance of a material. Talc particles play dual roles in scratch resistance. Talc improves scratch hardness by enhancing the mechanical properties. However, the corresponding scratch visibility increases significantly due to the massive formation of voids and exposed talc particles on the scratched surface. The approach to the reduction of scratch visibility can thus be partially answered. Preventing the material from reaching a deleterious mode

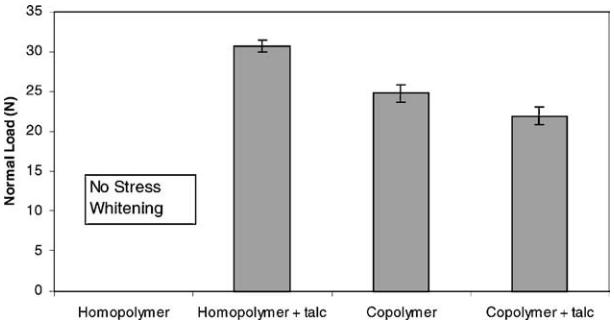


*Figure 18* Critical load to onset of stress-whitening.

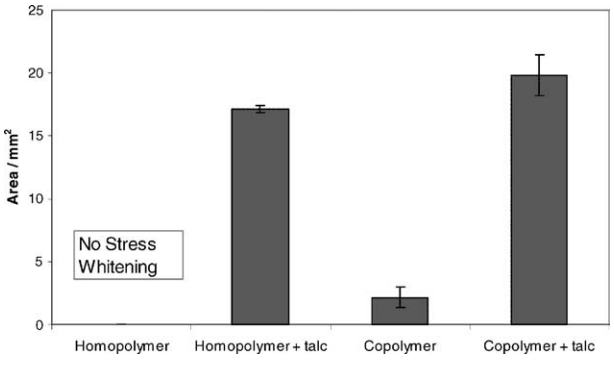


*Figure 19* Area of scratch groove that was stress-whitened.

of failure, i.e., extensive fibrillation of the matrix or talc debonding, should reduce scratch visibility. This can be achieved by improving interfacial adhesion between the talc particle and polymer matrix, by reducing the size of talc particles, or by increasing the yield strength and stiffness of PP.

For comparison, a gray level analysis of scratch visibility via scanner method is presented (Fig. 20). A graph of the gray levels of the unscratched surface was plotted to contrast with that of the scratch groove. The graph of the unscratched surface remains constant throughout the scratch length, while the scratch groove shows a gradual increase in gray level. Owing to the fact that the low resolution scanner can show only a monotonic increase in light intensity without any prominent peaks or change in value, it will not be very useful in characterizing scratch visibility.

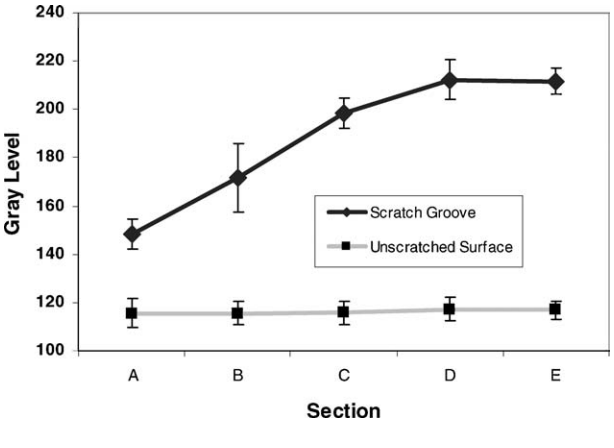


*Figure 20* Gray level plot of scanned image of a copolymer *via* flatbed scanner.

### *3.6.2. Ductile vs. brittle failure*

The present work suggests that stress-whitening during scratching is mainly due to the voiding, cracking, and ductile drawing of the scratched polymer. The ductile drawing is caused by void formation and debonding of rubber phase and talc particles from the matrix. Evidence of large tracts of material being removed (spalling) can also be seen in Figs 10c and 11b. In contrast, materials that failed in a localized brittle manner, i.e., homopolymer and talc-filled homopolymer, display minimal stress-whitening. Previous work done by other authors, such as Lin *et al*. [42] and Bertrand-Lambotte *et al*. [10], suggest that brittle failure will increase scratch visibility. It is reasoned that brittle failure will increase surface roughness of the scratch groove because of the formation of cracks, while ductile failure gives a smooth polished surface. Subsequently, as the eye is more sensitive to the change in surface roughness, scratch visibility is increased. However, it must be noted that the aforementioned authors came to this conclusion from scratch tests done on automotive clearcoats that produce scratch deformation in the microscale range up to 20 $\mu$m. Thenceforth, it is applicable to situations where marring occurs, an example being mars produced by minuscule sand particles. In the present case, where the dominant mechanism that produces large surface roughness is ductile drawing, voiding and debonding, a diametrically opposite conclusion is obtained. These contrasting conclusions show that scratch visibility cannot be described as simply related to ductile or brittle failure. The effect of the mode of failure to scratch visibility is sensitive to the type of material, inclusion phase and size, and possibly size of the scratches.

## 4. Conclusions

The progressive load test method is found to be useful in characterizing scratch behavior of polymers. Various surface damage features can be observed as the scratch progresses under the linear load increase condition. The surface damage transitions, such as mar-scratch and stress-whitening, can be correlated to transitions in the friction force profile and scratching coefficient of friction. Highly strained regions inside the scratch groove can be readily revealed using sonication. High fidelity of the friction force profile to the observed surface damage using SEM is demonstrated. Significant damage features found in SEM can always be corroborated to the peaks in the friction force profile. Talc, if not properly modified, is found to have a deleterious role in terms of scratch visibility, even though it increases the scratch hardness of PP. It is possible to reduce scratch visibility by suppressing undesirable failure mechanisms during scratch. Approaches for making scratch resistant polymers have been discussed.

## Acknowledgements

The authors would like to acknowledge valuable insights from discussions with Mr. G.T. Lim. The authors would like to acknowledge the financial support provided by the Texas A&M Scratch Behavior

Consortium (Advanced Composites—Brian Coleman, BP Chemical—Kathryn Shuler, Luzenac—Richard Clark, Solvay Engineered Polymers—Edmund Lau, Visteon—Beth Wichterman and Rose Ryntz), the State of Texas (ARP #32191-73130) and Defense Logistic Agency (SP0103-02-D-0003) in this research endeavor. Special thanks are given to the Japanese collaborators H. Kita of National Institute of Testing and Evaluation and M. Kotaki, T. Kuriyama, and T. Inoue of Yamagata University for their insightful discussions. Special thanks are also given to the Society of Plastics Engineers—South Texas Section for their generous donation of equipment and Atlas Material Testing Technology for their loan of optical imaging equipment, VIEEW®, for this research.

## References

1. I. M. HUTCHINGS, *Mater. Sci. Eng.* A **184** (1994) 185.
2. F. P. BOWDEN and D. TABOR, in "The Friction and Lubrication of Solids," Part I (Oxford University Press, Oxford, 1950) p. 33.
3. F. P. BOWDEN and D. TABOR, in "The Friction and Lubrication of Solids," Part II (Oxford University Press, Oxford, 1964) p. 350.
4. K. LI, B. Y. NI and J. C. M. LI, *J. Mater. Res.* **11** (1996) 1574.
5. B. Y. NI and A. L. FAOU, *J. Mater. Sci.* **31** (1996) 3955.
6. H. BREUER, F. HAAF and J. STABENOW, *J. Macromol. Sci.— Phys.* B **14** (1977) 387.
7. J. HOLOUBEK and M. RAAB, *Collect. Czech. Chem. Commun.* **60** (1995) 1875.
8. B. J. BRISCOE, E. PELILLO and S. K. SINHA, *Polymer Eng. Sci.* **36** (1996) 2996.
9. B. J. BRISCOE, P. D. EVANS, S. K. BISWAS and S. K. SINHA, *Tribol. Intern.* **29** (1996) 93.
10. P. BERTRAND-LAMBOTTE, J. L. LOUBET, C. VERPY and S. PAVAN, *Thin Solid Films* **420/421** (2002) 281.
11. M. WONG, G. T. LIM, A. MOYSE, J. N. REDDY and H.-J. SUE, *Wear*, in press.
12. A. G. ATKINS and Y.-W. MAI, "Elastic and Plastic Fracture—Metals, Polymers, Ceramics, Composites, Biological Materials" (Ellis Horwood Ltd., Chichester, 1985) p.758.
13. H. TANG and D. C. MARTIN, *J. Mater. Sci.* **38** (2003) 803.
14. C. XIANG, H.-J. SUE, J. CHU and B. COLEMAN, *J. Polym. Sci. B: Polym. Phys.* **39** (2001) 47.
15. B. J. BRISCOE, E. PELILLO and S. K. SINHA, *Polym. Intern.* **43** (1997) 359.
16. R. S. KODY and D. C. MARTIN, *Polym. Eng. Sci.* **36** (1996) 298.
17. J. R. GRASMEDER, in Polypropylene, the International Conference (Institute of Materials, London, 1994) p. 98.
18. P. Z. WANG, I. M. HUTCHINGS, S. J. DUNCAN and L. JENKINS, *SAE Trans.* **1999-01-0243** (1999) 134.
19. P. RANGARAJAN, M. SINHA, V. WATKINS and K. HARDING, *Polym. Eng. Sci.* **43** (2003) 749.
20. D 618-00, Annual Book of ASTM Standards (2003) Vol. 8.01. p. 35.
21. V. JARDRET, B. N. LUCAS, W. C. OLIVER and A. C. RAMAMURTHY, *J. Coats. Tech.* **72** (2000) 79.
22. J. J. GILMAN, in "The Science of Hardness Testing and Its Research Applications," Detroit, Oct. 1971, edited by J. H. Westbrook and H. Conrad (American Society for Metals, Metals Park, 1973) p. 51.
23. D. TABOR, in "The Hardness of Metals" (Oxford University Press, Oxford, 1951) p.6.
24. B. J. BRISCOE and K. S. SEBASTIAN, *Proc. R. Soc. Lond.* A **452** (1996) 439.
25. M. SAKAI and Y. NAKANO, *J. Mater. Res.* **17** (2002) 2161.
26. A. C.-M. YANG and T. W. WU, *J. Polym. Sci. B: Polym Phys.* **35** (1997) 1295.
27. R. RIKARDS and A. FLORES, *J. Macromol. Sci. Phys.* B **40** (2001) 763.
28. R. RODRÍGUEZ and I. GUTIERREZ, *Mater. Sci. Eng.* A **361** (2003) 377.
29. W. D. NIX and H. GAO, *J. Mech. Phys. Solids* **46** (1998) 411.
30. H. VAN MELICK, A. VAN DIJKEN, J. DEN TOONDER, L. GOVAERTY and H. MEIJERY, *Philo. Mag.* A **82** (2002) 2093.
31. F. YANG, J. Y. ZHOU, V. KORDONSKI and S. D. JACOBS, *J. Mater. Sci. Lett.* **15** (1996) 1523.
32. M. SAKAI, *J Mater. Res.* **14** (1999) 3630.
33. Y.-T. CHENG and C.-M. CHENG, *Surf. Coat. Tech.* **133/134** (2000) 417.
34. H. C. Y. CARTLEDGE, C. BAILLIE and Y.-W. MAI, *Wear* **194** (1996) 178.
35. C. PISTOR and K. FRIEDRICH, *J. Appl. Polym. Sci.* **66** (1997) 1985.
36. J. CHU, C. XIANG, H.-J. SUE and R. DAMON HOLLIS, *Polym. Eng. Sci.* **40** (2000) 944.
37. J. CHU, L. RUMAO and B. COLEMAN, *ibid.* **38** (1998) 1906.
38. A. DASARI, J. ROHRMANN and R. D. K. MISRA, *Macromol. Mater. Eng.* **287** (2002) 889.
39. D. RATS, V. HAJEK and L. MARTINU, *Thin Solid Films* **340** (1999) 33.
40. N. G. MCCRUM, C. P. BUCKLEY and C. B. BUCKNALL, in "Principles of Polymer Engineering," 2nd ed. (Oxford Science Publications, Oxford, 1999) p.186.
41. R. RENGARAJAN, S.K. KESAVAN, K. L. FULLERTON and S. LEE, *J Appl. Polym. Sci.* **45** (1992) 317.
42. L. LIN, G. S. BLACKMAN and R. R MATHESON, in "Microstructures and Microtribology of Polymer Surfaces," Boston, August 1998, edited by V. V. Tsukruk and K. L. Wahl (ACS, Washington D. C, 2000) p. 428.

*Received 20 August 2003*
*and accepted 12 January 2004*